Electronic Supplementary Material (ESI) for RSC Advances.

Supporting Information

A single fluorescent chemosensor for multiple targets Cu^{2+}, $Fe^{2+/3+}$ and Al^{3+} in living cells and a near-perfect aqueous solution

Tae Geun Jo,[a] Jae Min Jung,[a]* Jiyeon Han,[b] Mi Hee Lim,[b] Cheal Kim[a]*

[a]*Department of Fine Chemistry and Department of Interdisciplinary Bio IT Materials, Seoul National University of Science and Technology, Seoul 139-743, Republic of Korea. Fax: +82-2-973-9149; Tel: +82-2-970-6693; E-mail: iamjemin@naver.conm and chealkim@seoultech.ac.kr*

[b]*Department of Chemistry, Ulsan National Institute of Science and Technology (UNIST), Ulsan 44919, Republic of Korea.*

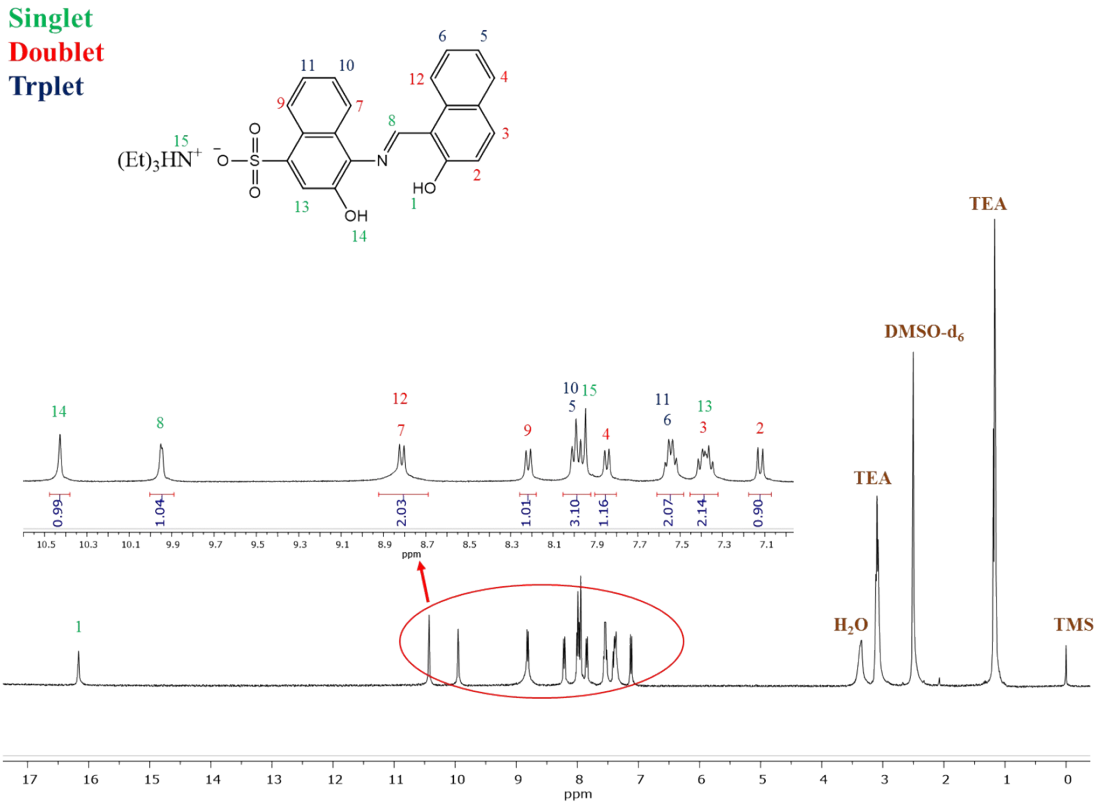

Fig. S1 ^{1}H NMR spectrum of **1** in DMSO-d_6.

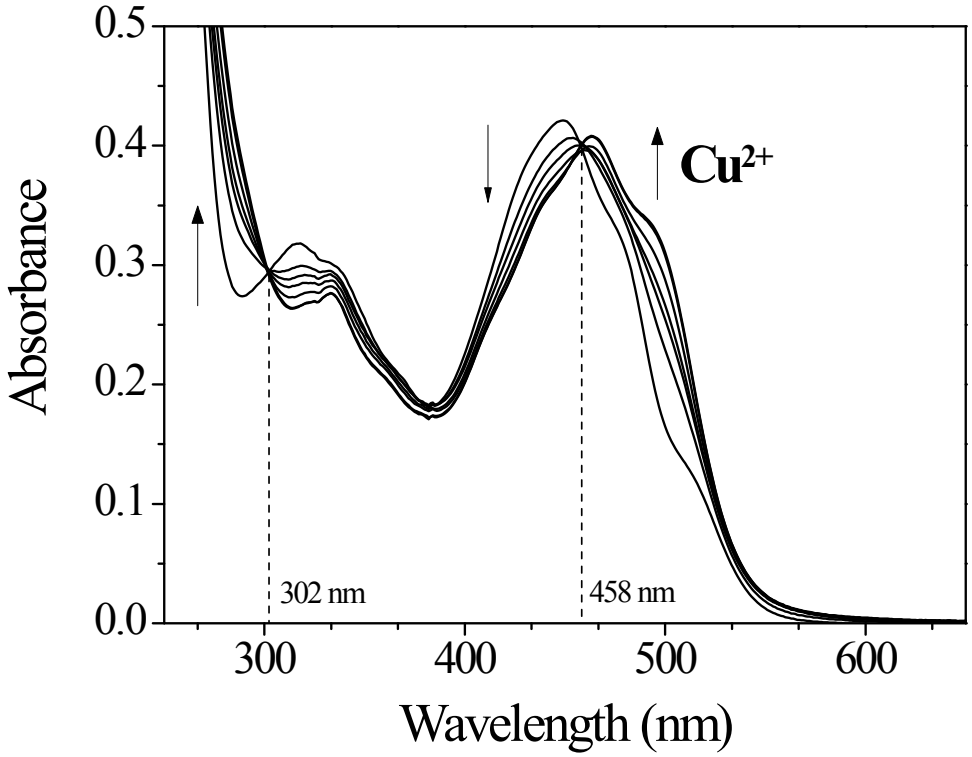

Fig. S2 UV-vis spectral change of **1** (30 μM) with Cu^{2+} ions (0-1 equiv) in bis-tris buffer (10 mM, pH 7.0).

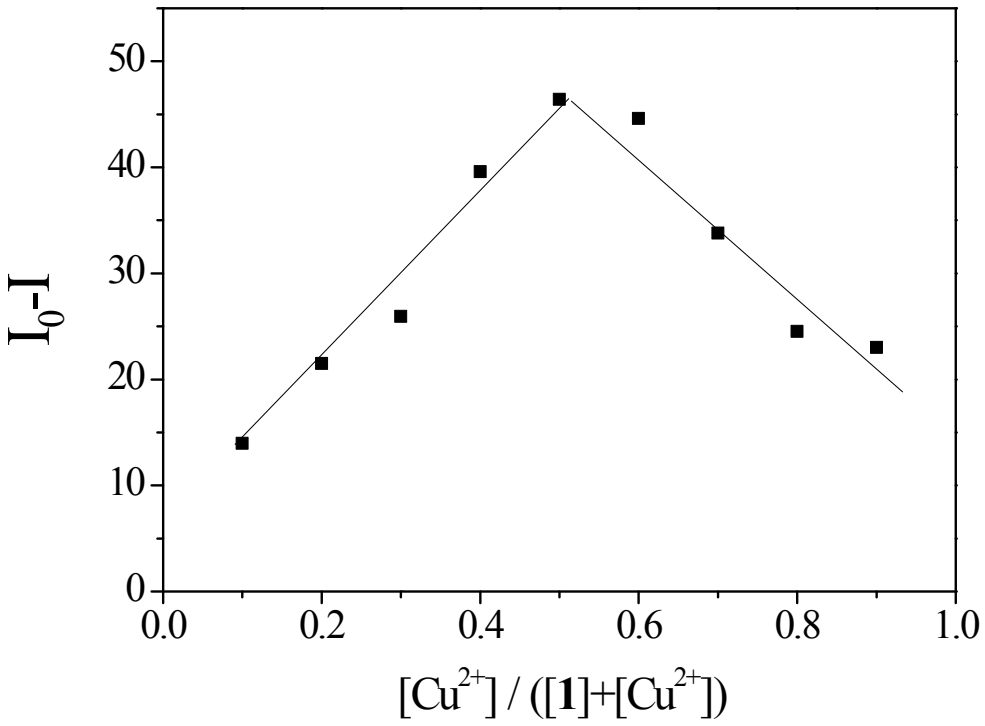

Fig. S3 Job plot of **1** (30 μM) with Cu^{2+}, where the intensity at 442 nm was plotted against the mole fraction of Cu^{2+}.

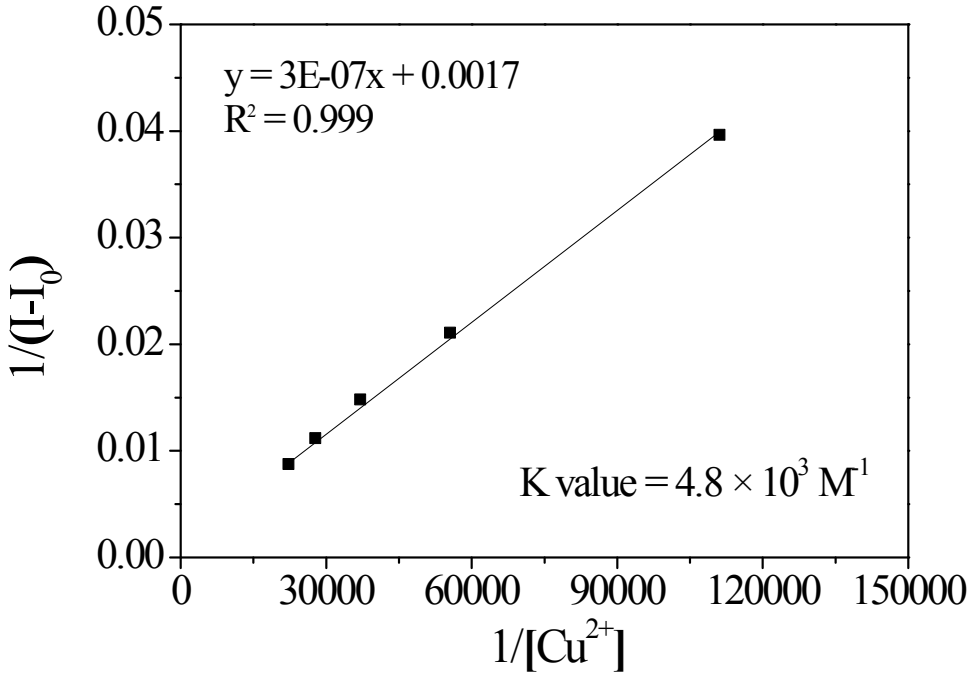

Fig. S4 Benesi-Hildebrand plot of **1** (30 μM) for Cu^{2+}, assuming 1:1 stoichiometry for association of **1** with Cu^{2+}.

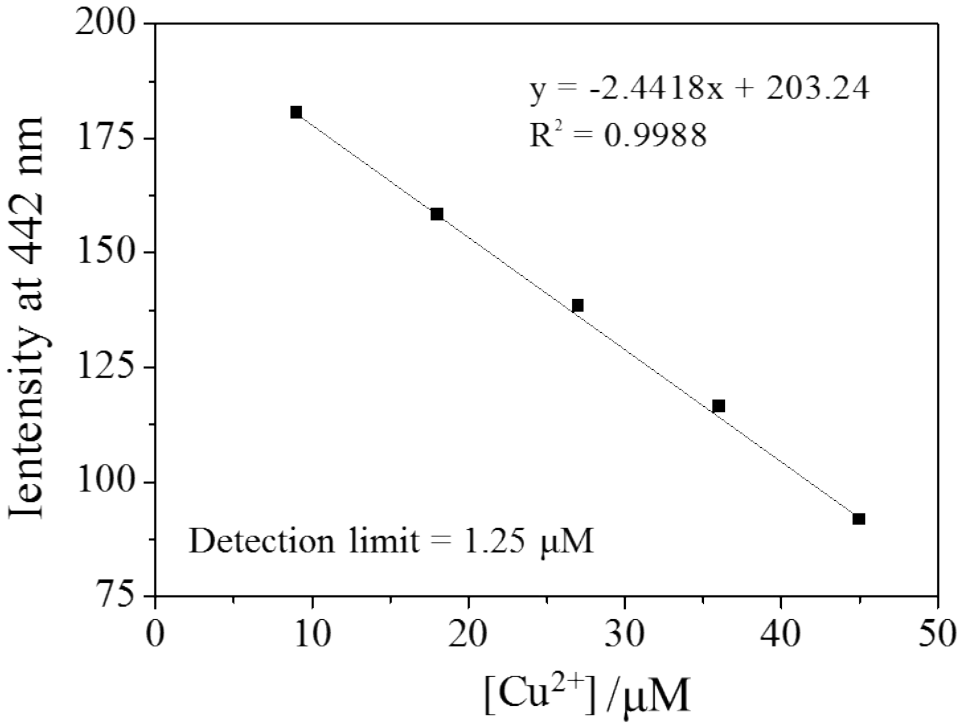

Fig. S5 Determination of the detection limit of **1** (30 μM) for Cu^{2+} based on change of intensity at 442 nm.

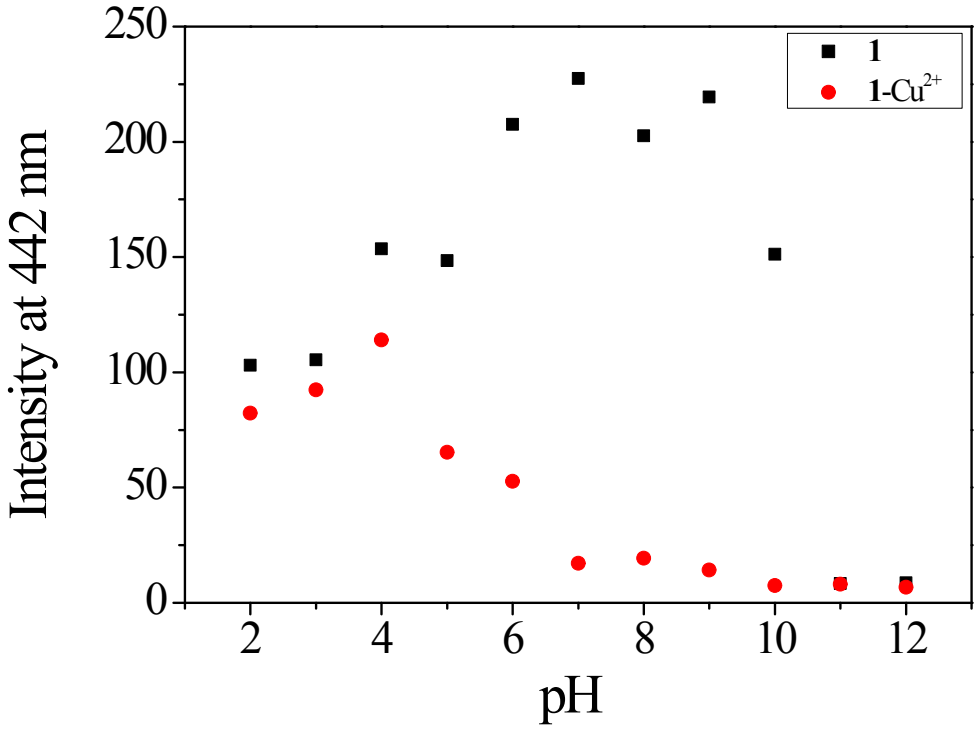

Fig. S6 Fluorescence intensities (at 442 nm) of **1** (30 μM) and **1**-Cu^{2+} complex in different pH (2-12) solutions (bis-tris buffer, 10 mM).

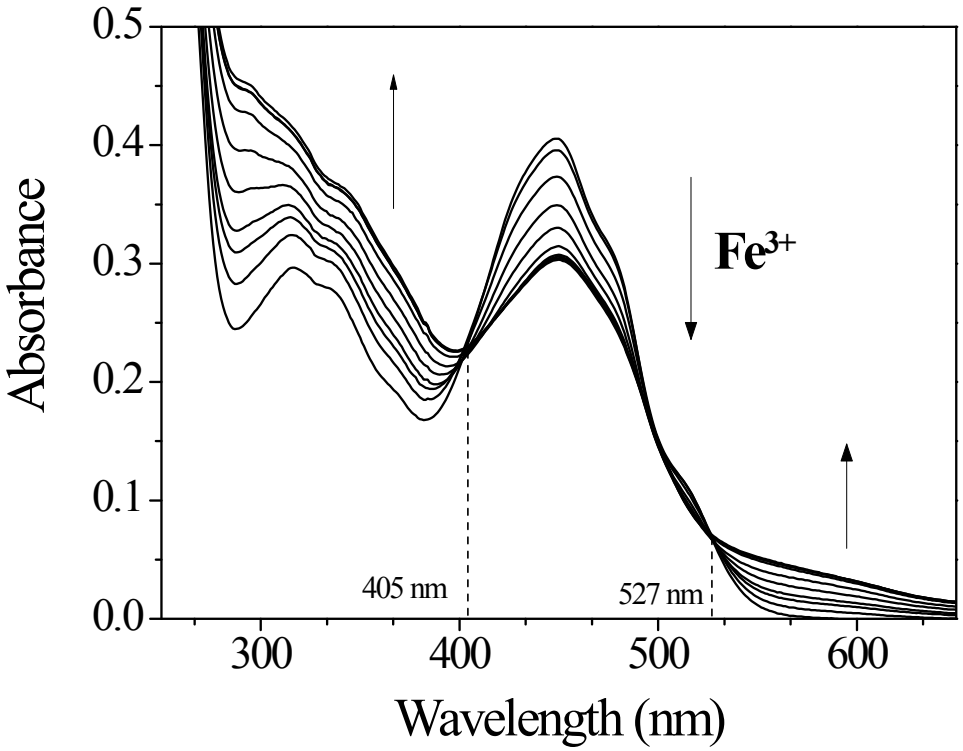

Fig. S7 UV-vis spectral changes of **1** (30 μM) with Fe^{3+} ions (0-1 equiv) in bis-tris buffer (10 mM, pH 7.0).

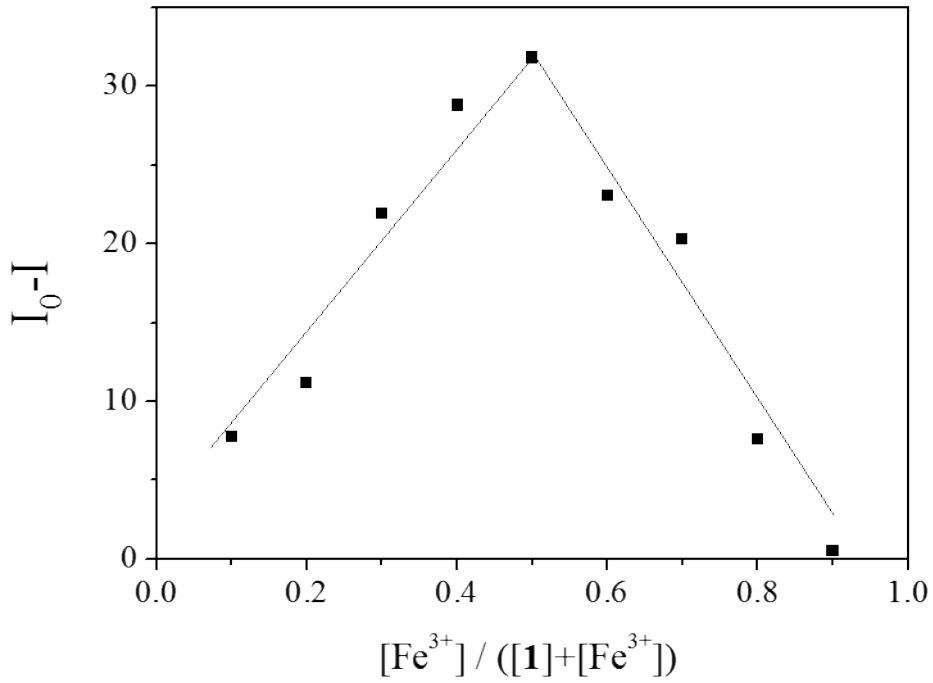

Fig. S8 Job plot of **1** (30 μM) with Fe^{3+}, where the intensity at 442 nm was plotted against the mole fraction of Fe^{3+}.

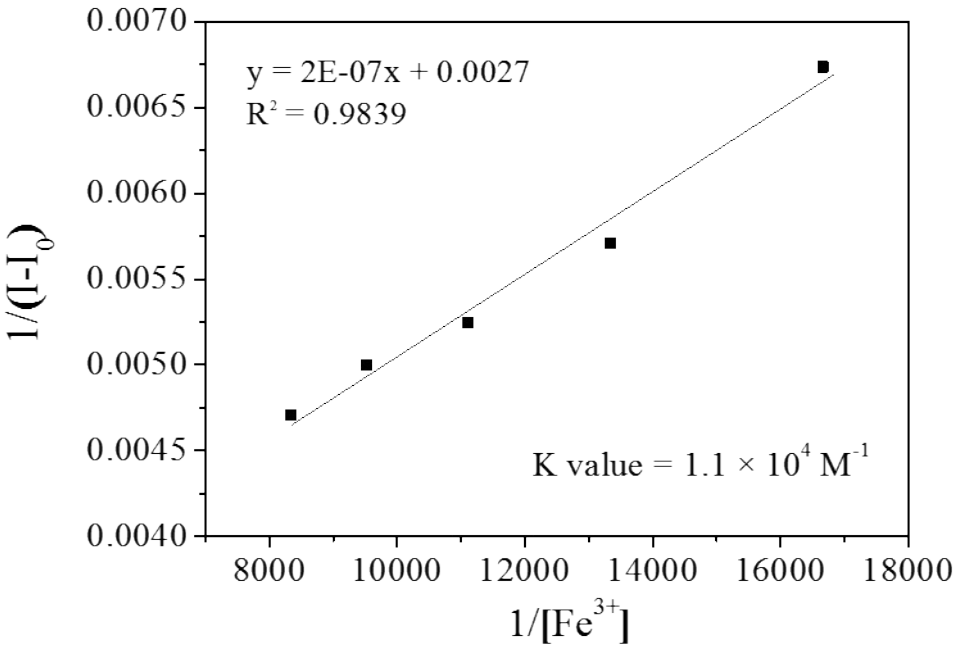

Fig. S9 Benesi-Hildebrand plot of **1** (30 μM) for Fe^{3+}, assuming 1:1 stoichiometry for association of **1** with Fe^{3+}.

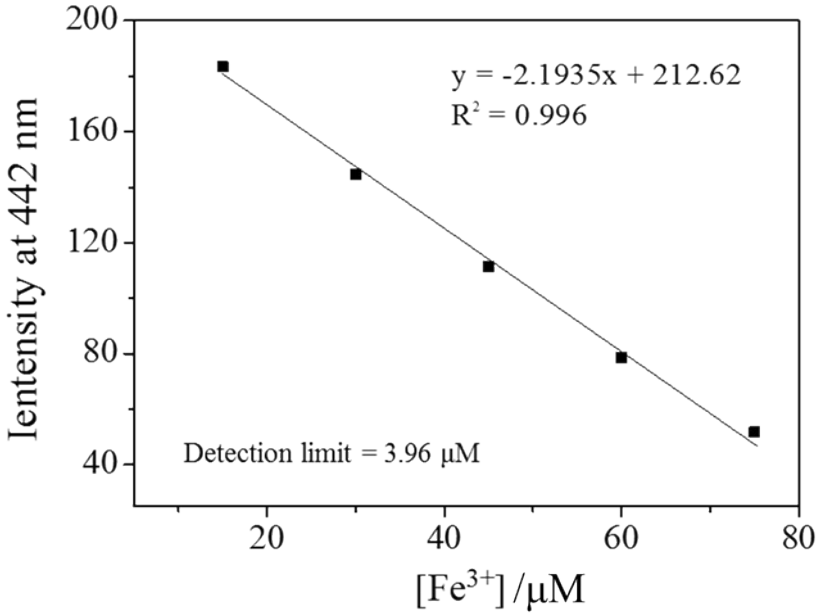

Fig. S10 Determination of the detection limit of **1** (30 μM) for Fe^{3+} based on change of intensity at 442 nm.

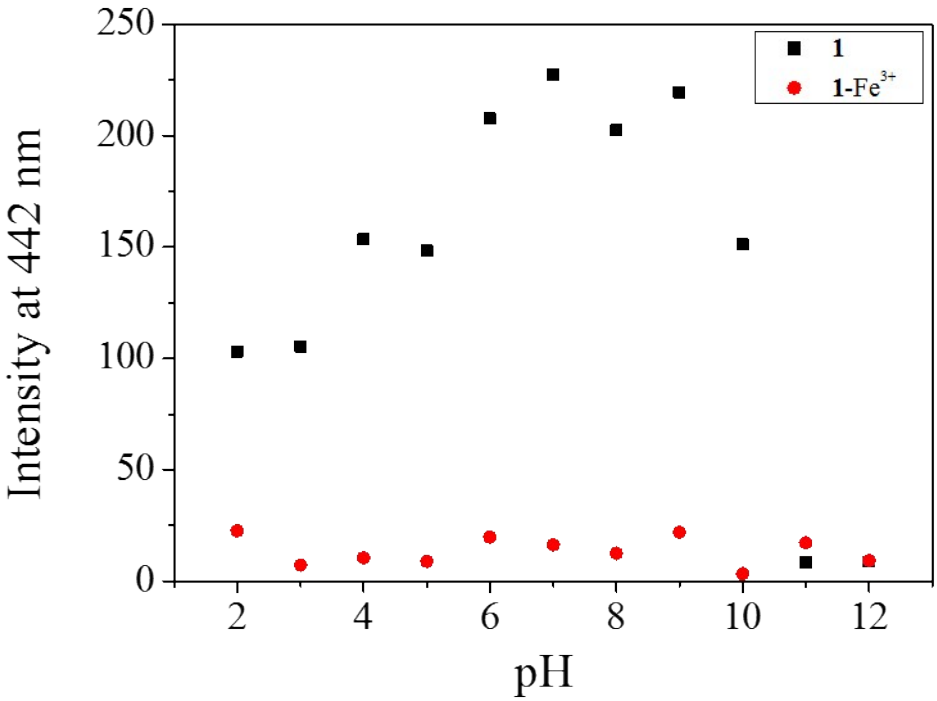

Fig. S11 Fluorescence intensities (at 442 nm) of **1** (30 μM) and **1**-Fe^{2+} complex in different pH (2-12) solutions (bis-tris buffer, 10 mM).

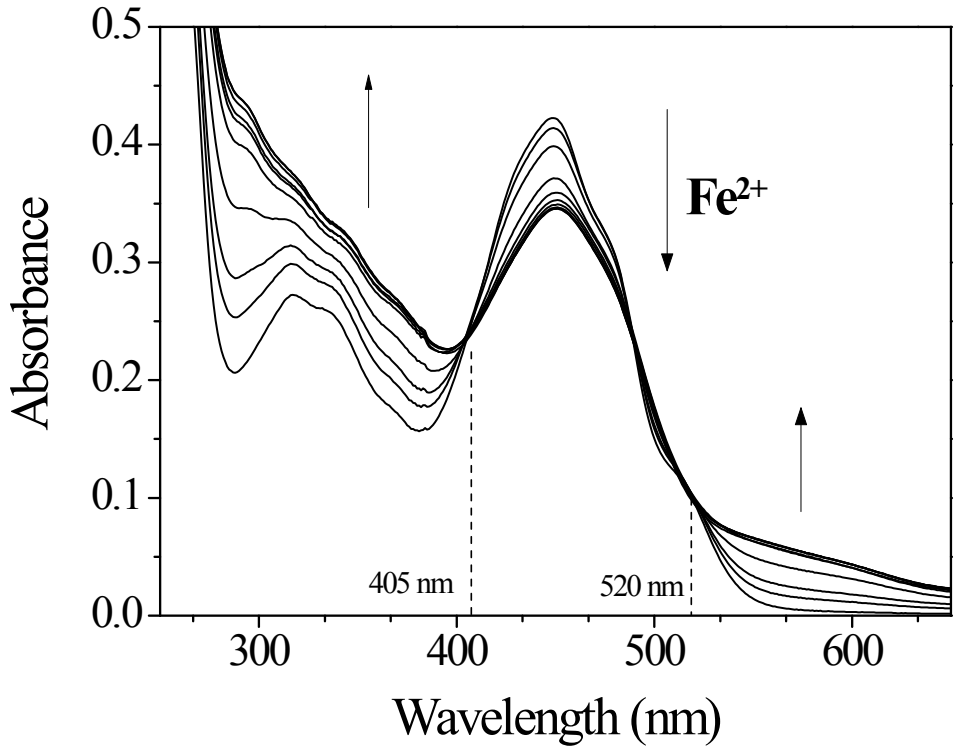

Fig. S12 UV-vis spectral changes of **1** (30 μM) with Fe^{2+} ions (0-1 equiv) in bis-tris buffer (10 mM, pH 7.0).

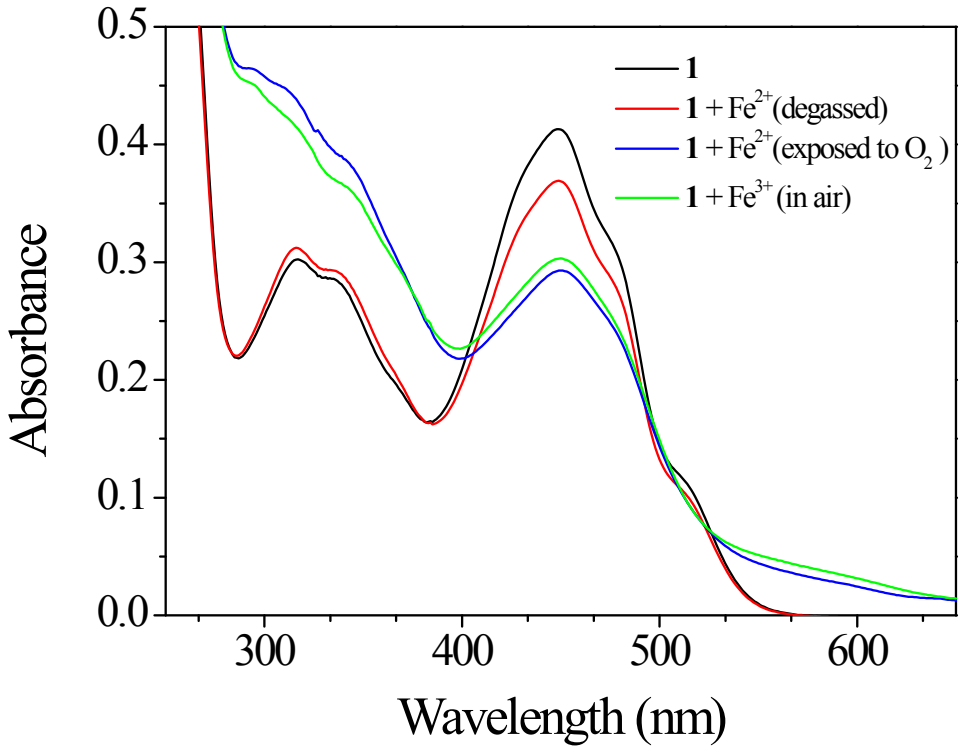

Fig. S13 UV-vis spectral changes of **1** (30 μM) with Fe^{2+} under the degassed and aerobic conditions, respectively.

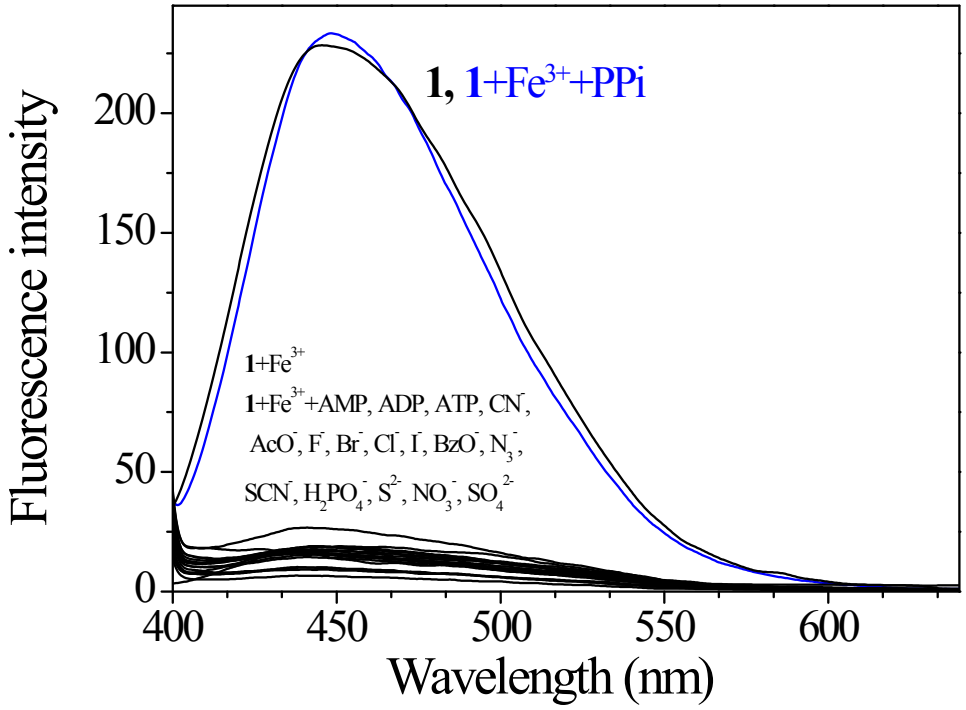

Fig. S14 Fluorescence spectra of **1**-Fe^{3+} (30 μM) upon addition of 20 equiv of different anions in buffer (10 mM bis-tris, pH 7.0).

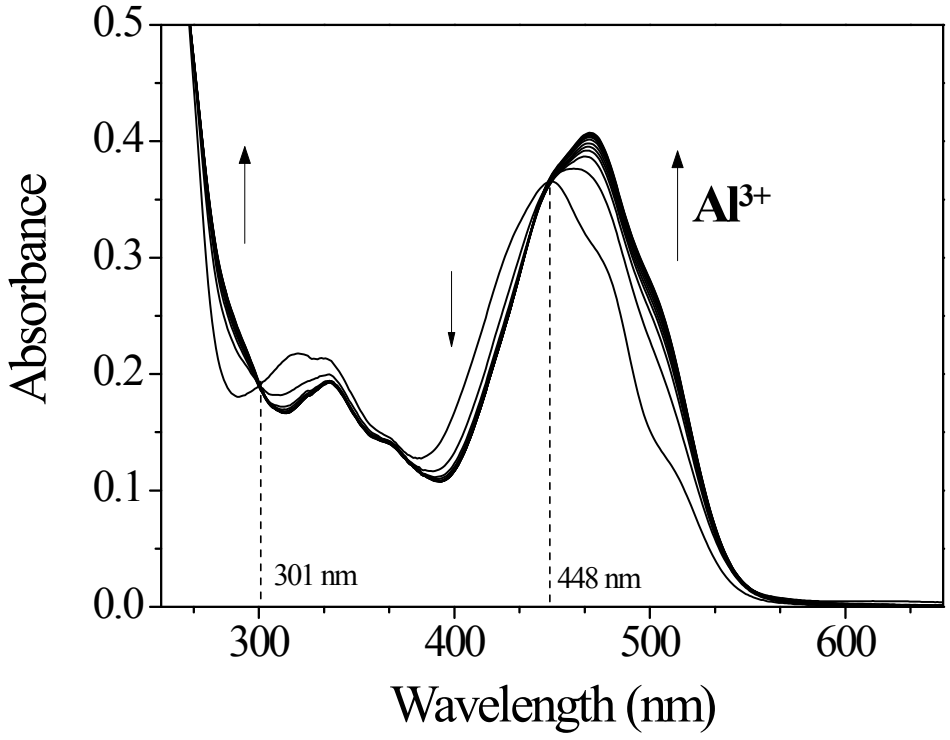

Fig. S15 UV-vis spectral changes of **1** (30 μM) with Al^{3+} ions (0-75 equiv) in bis-tris buffer (10 mM, pH 7.0).

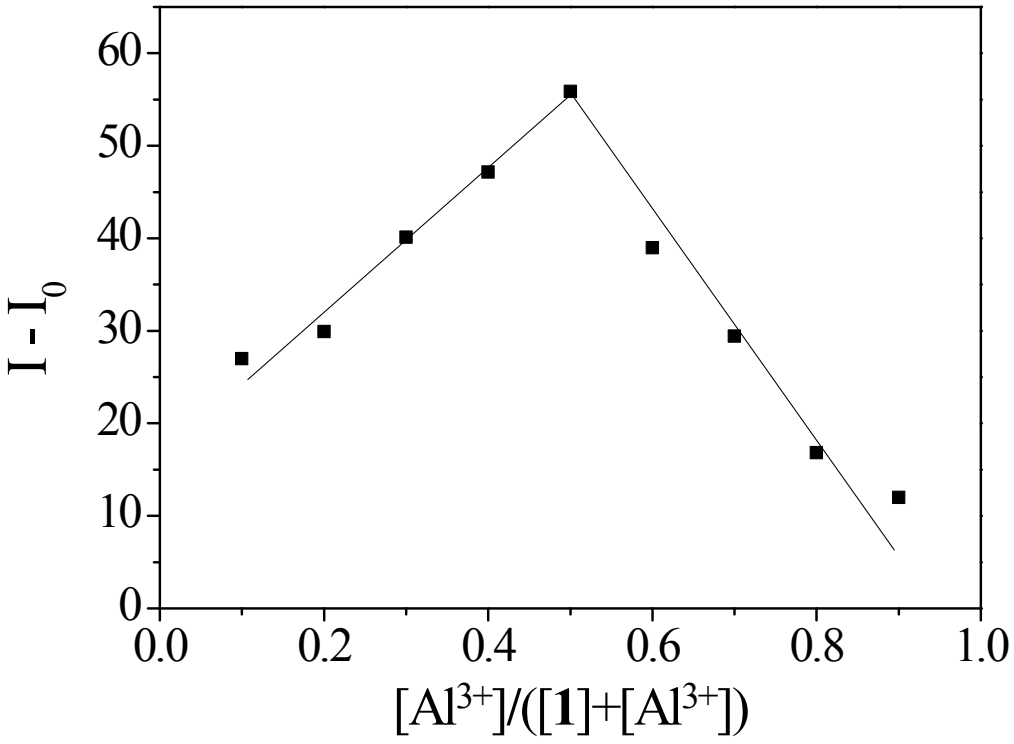

Fig. S16 Job plot of **1** (30 μM) with Al^{3+}, where the intensity at 535 nm was plotted against the mole fraction of Al^{3+}.

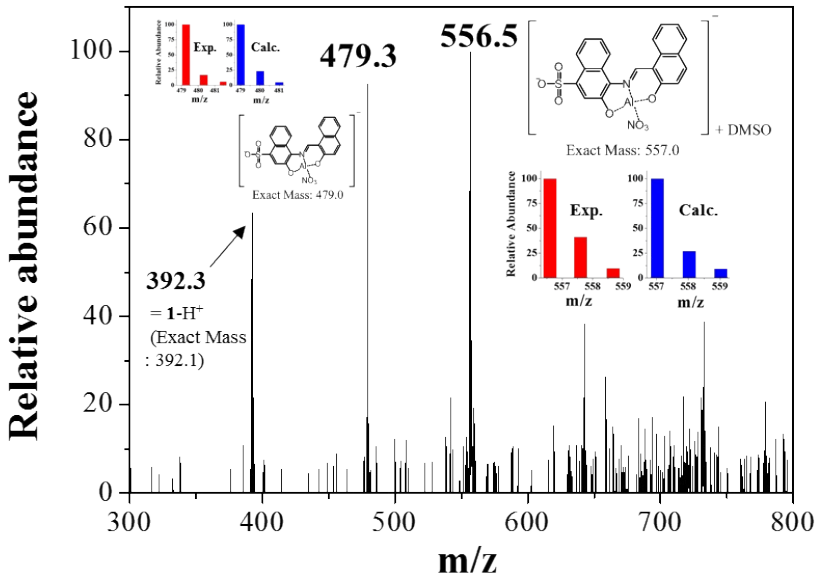

Fig. S17 Negative-ion ESI-mass spectrum of **1** (100 μM) upon addition of 1 equiv of Al^{3+}.

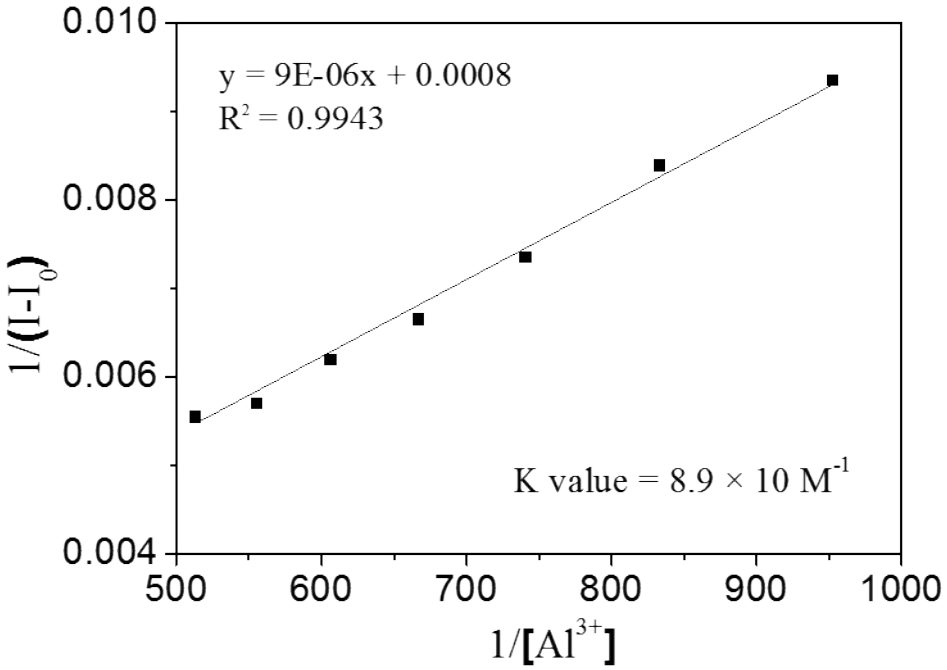

Fig. S18 Benesi-Hildebrand plot of **1** (30 μM) for Al^{3+}, assuming 1:1 stoichiometry for association of **1** with Al^{3+}.

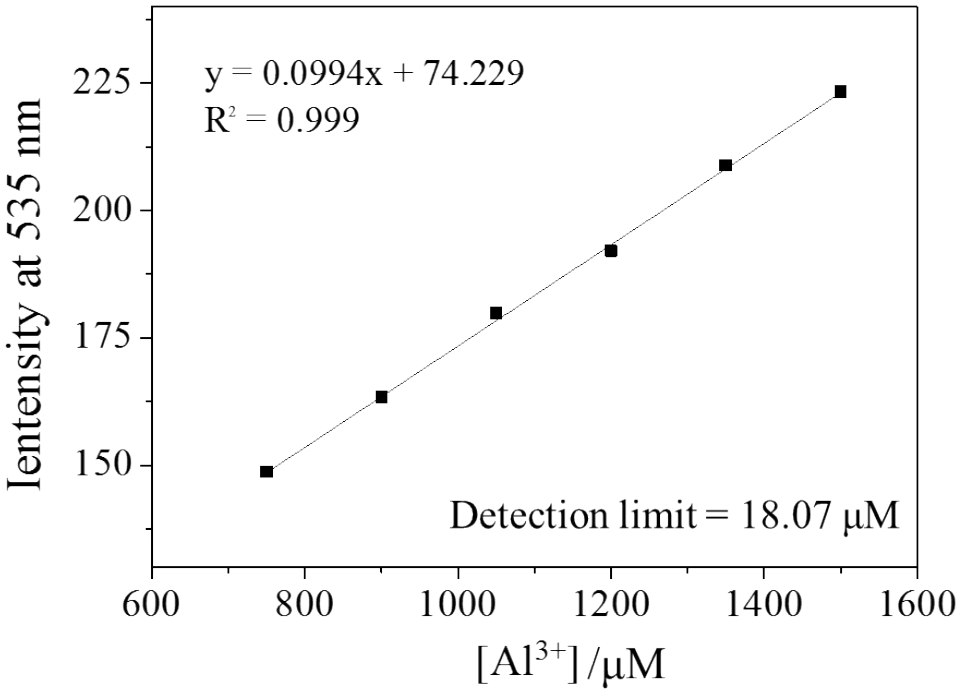

Fig. S19 Determination of the detection limit of **1** (30 μM) for Al^{3+} based on change of intensity at 535 nm.

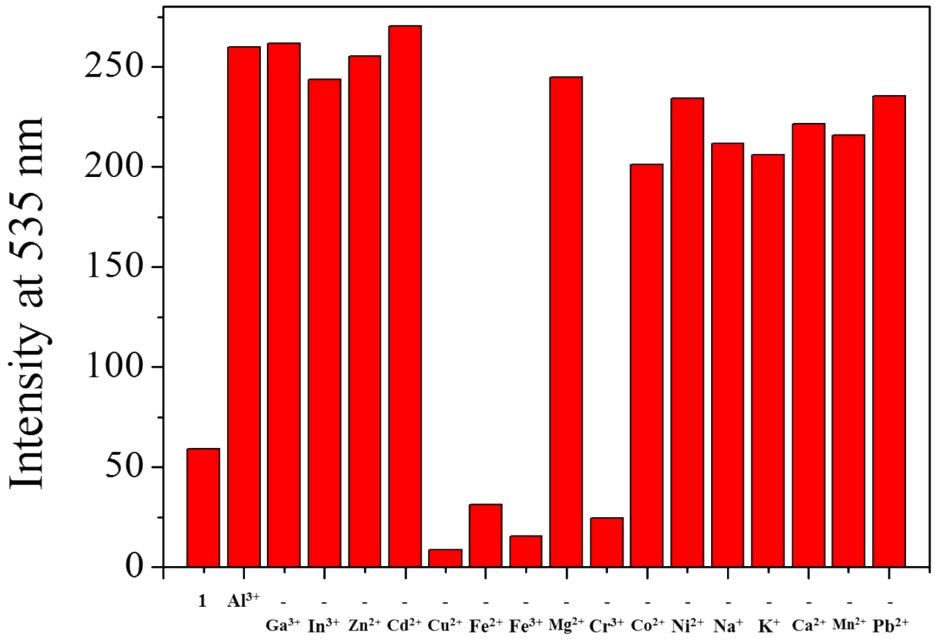

Fig. S20 Fluorescence intensities (at 535 nm) of **1** (30 μM) upon addition of Al^{3+} (70 equiv) in the absence and presence of other metal ions (70 equiv).

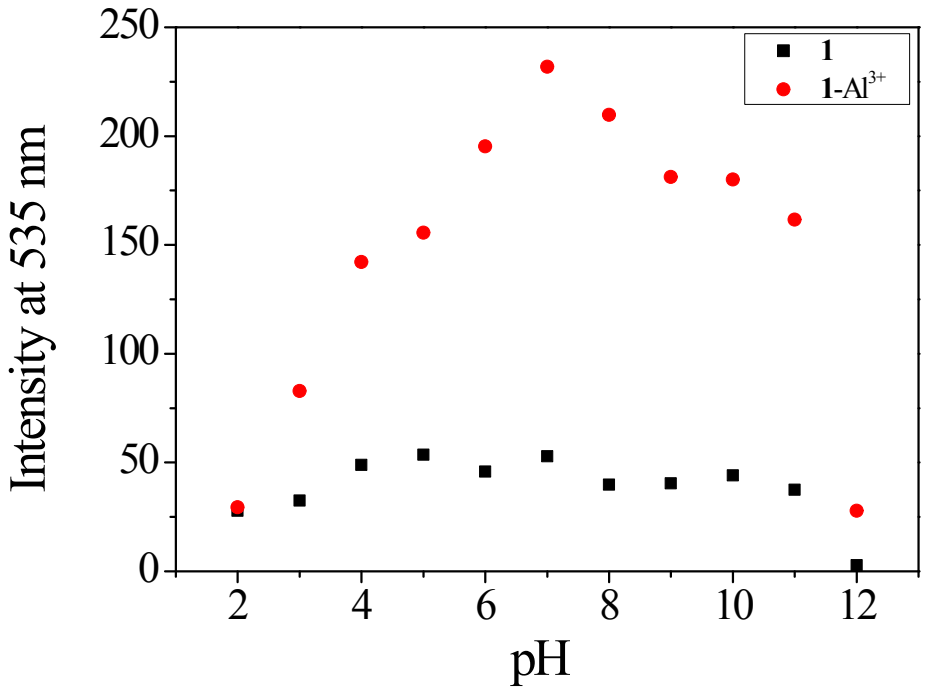

Fig. S21 Fluorescence intensities (at 535 nm) of **1** (30 μM) and **1**-Al^{3+} complex in different pH (2-12) solutions (bis-tris buffer, 10 mM).

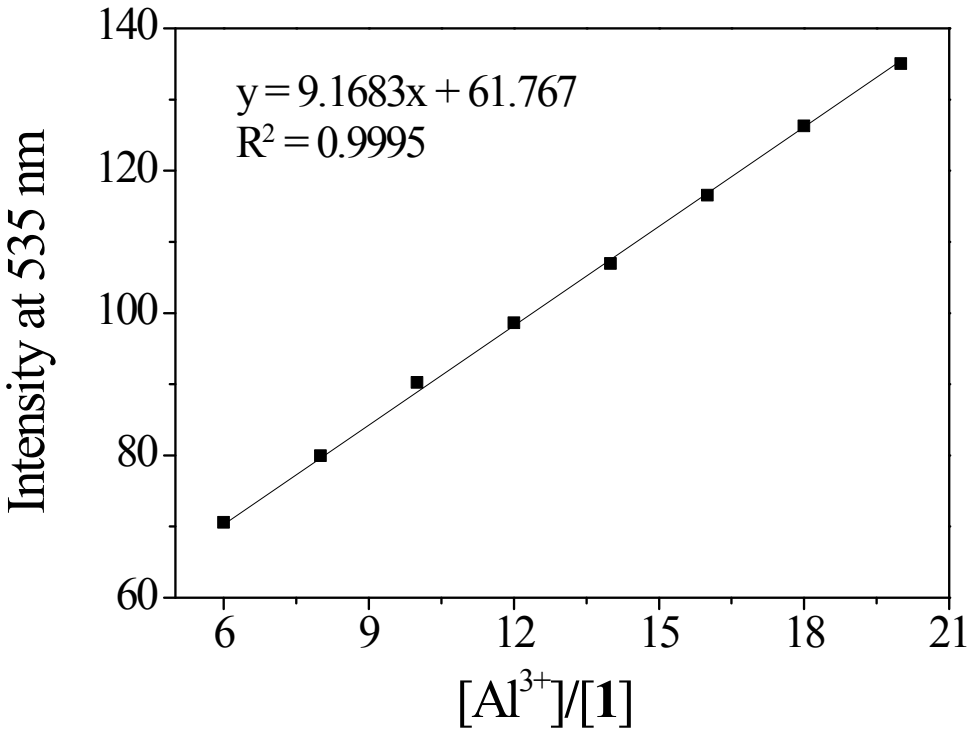

Fig. S22 Fluorescence intensities (at 535 nm) of **1** as a function of Al^{3+} concentration. [**1**] = 30 μM and [Al^{3+}] = 180-630 μM.

(a)

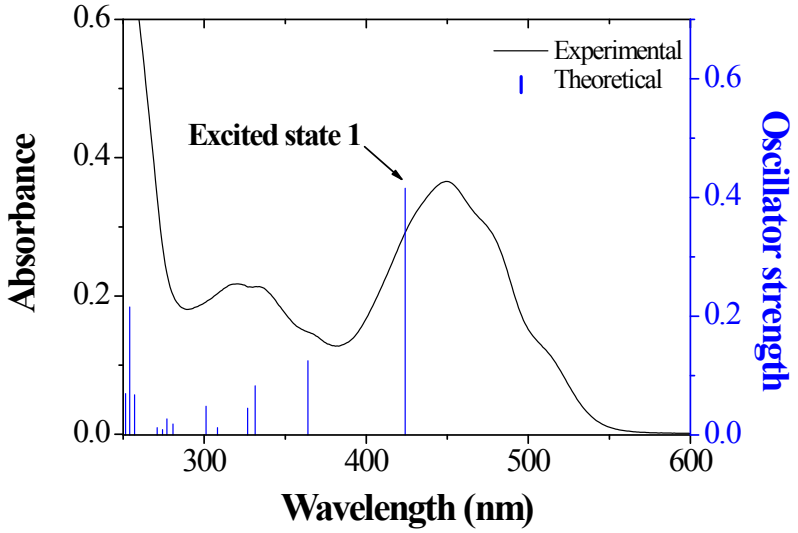

(b)

Excited State 1	Wavelength	Percent (%)	Character	Oscillator strength
H → L	424.0	95%	ICT	0.4156

(c)

Molecular orbital (1)	
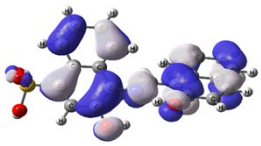	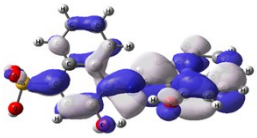
HOMO (-5.700 eV)	LUMO (-2.236 eV)

Fig. S23 (a) The theoretical excitation energies (TD-DFT method) and the experimental UV-vis spectrum of **1**. (b) The major electronic transition energy and molecular orbital contribution for **1** (H = HOMO and L = LUMO). (c) Isosurface (0.030 electron bohr-3) of molecular orbitals participating in the major singlet excited state of **1**.

(a)

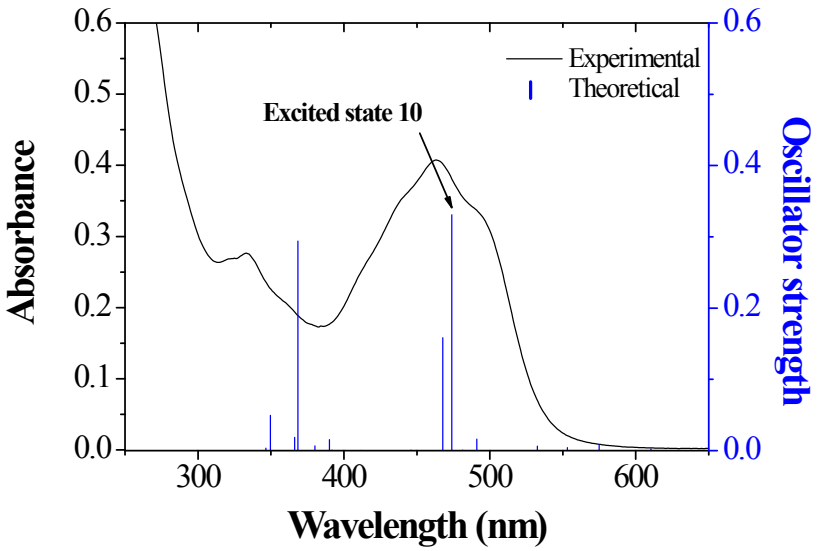

(b)

Excited State 10	Wavelength	percent (%)	Character	Oscillator strength
H (α) → L (α)	474.0	29%	ICT	0.3310
H (β) → L+1 (β)		28%	ICT	
H-3 (β) → L (β)		4%	LMCT	
H-6 (β) → L (β)		5%	LMCT	
H-7 (β) → L (β)		2%	LMCT	
H-13 (β) → L (β)		3%	LMCT	
H-16 (β) → L (β)		2%	LMCT	
H-17 (β) → L (β)		2%	LMCT	
H-19 (β) → L (β)		2%	LMCT	
H-21 (β) → L (β)		8%	LMCT	

(c)

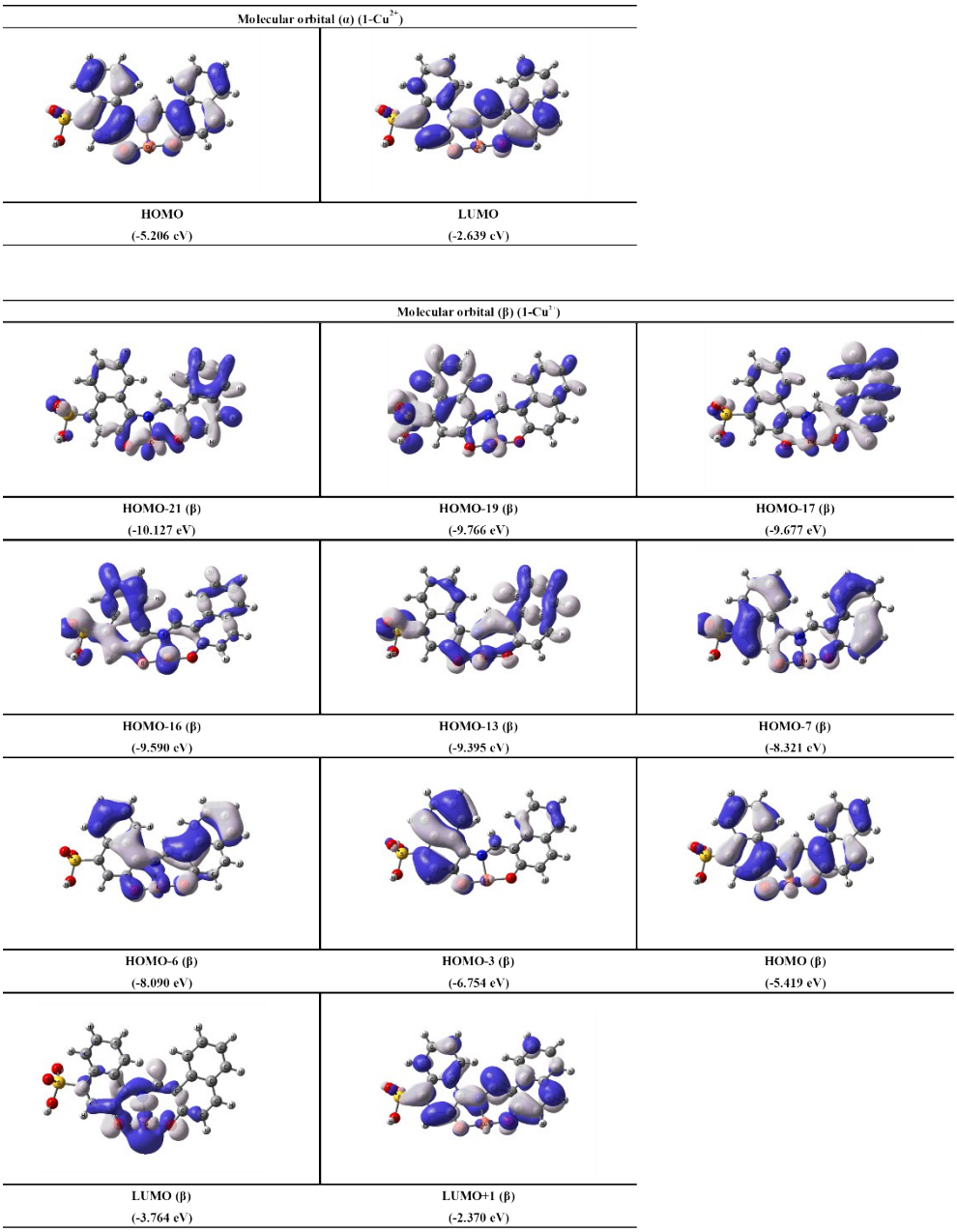

Fig. S24 (a) The theoretical excitation energies (TD-DFT method) and the experimental UV-vis spectrum of **1**-Cu^{2+}. (b) The major electronic transition energies and molecular orbital contributions for **1**-Cu^{2+} (H = HOMO and L = LUMO). (c) Isosurface (0.030 electron bohr-3) of molecular orbitals participating in the major singlet excited state of **1**-Cu^{2+}.

(a)

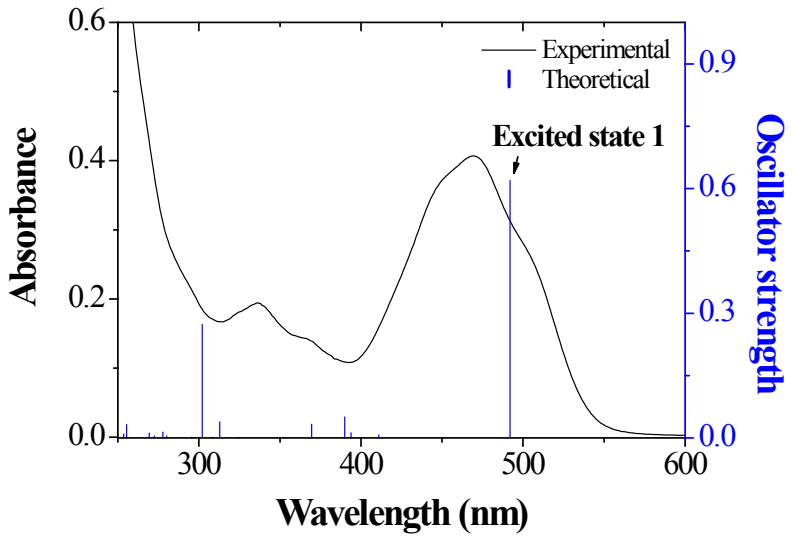

(b)

Excited State 1	Wavelength	percent (%)	Character	Oscillator strength
H → L	492.0	99%	ICT	0.6196

(c)

Molecular orbital (1-Al^{3+})	
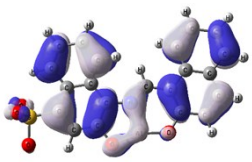	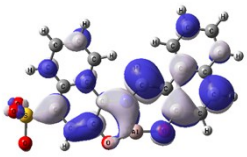
HOMO (-6.336 eV)	LUMO (-3.407 eV)

Fig. S25 (a) The theoretical excitation energies (TD-DFT method) and the experimental UV-vis spectrum of **1**-Al^{3+}. (b) The major electronic transition energy and molecular orbital contribution for **1**-Al^{3+} (H = HOMO and L = LUMO). (c) Isosurface (0.030 electron bohr-3) of molecular orbitals participating in the major singlet excited state of **1**-Al^{3+}.